Thermochimica Acta 740 (2024) 179828

Contents lists available at ScienceDirect

Thermochimica Acta

journal homepage: www.elsevier.com/locate/tca

Effects of external static electrical field on thermal and electrical conductivity in the Al-Cu, Al-Ni, and Al-Si eutectic alloys

Sercan Basit [a], Pınar Ata Esener [b,*], Yiğit Yavuz Aydoğan [c], Sezen Aksöz [d], Necmettin Maraşlı [e]

[a] Department of Mechanical Engineering, Kırşehir Ahi Evran University, Kırşehir, 40100, Turkey
[b] Graduate School of Natural and Applied Sciences, Erciyes University, Kayseri, 38280, Turkey
[c] Department of Metallurgical and Materials Engineering, Yıldız Teknik University, İstanbul, 50100, Turkey
[d] Department of Physics, Nevşehir Hacı Bektaş Veli University, Nevşehir, 50100, Turkey
[e] Department of Aeronautical Engineering, İstanbul Gelişim University, İstanbul, 34310, Turkey

ARTICLE INFO

Keywords:
Eutectic alloys
Solidification under electric field
Thermal conductivity
Electrical conductivity

ABSTRACT

This study aims to investigate the effects of external positive and negative static electric fields (E_+ and E_- respectively) on thermal conductivity (K) and electrical conductivity (σ) in Al-33 wt. % Cu, Al-6.4 wt. % Ni and Al-12 wt. % Si eutectic alloys. For this purpose, the solidifications of Al-Cu, Al-Ni, and Al-Si eutectic alloys were directionally done under E_+ and E_-. The directions of E were chosen to be parallel (E_+) and antiparallel (E_-) to the solid-liquid (S-L) growth direction and the magnitudes of E were approximately (+10) and (−10) kV cm^{-1} and (+16) and (-16) kV cm^{-1} for the Al-Cu, Al-Ni, and Al-Si eutectic alloys, respectively. The effects of E_+ and E_- on the K and σ were determined by the longitudinal heat flow and the four-point probe methods, respectively. While the K and σ values decreased with increasing temperature, the K and σ were increased and decreased with E_+ and E_-, respectively.

1. Introduction

Solidification, one of the fundamentals of casting technology, is the process of transforming materials from liquid to solid. This process is an important feature of many processes such as welding, surface alloying, ingot production, crystal growth, and material purification [1]. By solidifying binary or ternary eutectic alloys, the microstructure, electrical, thermal, and mechanical properties of the materials can be changed [2]. Eutectic alloys can produce castings with good properties due to their low melting point and good fluidity, as well as their excellent mold-filling ability. Therefore, solidified eutectic alloys have great value in the production of advanced structural materials [3–6].

Aluminum (Al) based alloys have been notable for their low density, high ductility, good corrosion resistance, high strength [7–9], and good thermal and electrical properties [10]. These alloys find applications in many fields such as construction, aviation, space, and automotive due to their lightness. Copper (Cu) is one of the metals with extremely high solubility in aluminum. Adding copper to aluminum lowers the melting point of the alloys while increasing the strength and heat treatability of the alloy. Effects such as chemical composition, cooling rate, and heat treatment can change the microstructure and mechanical properties of Al-Cu alloys [8,11,12]. Studies have shown that Al-Ni alloys have high melting points, good oxidation resistance, relatively low density, and excellent mechanical properties [13,14]. Al-Si alloys, like Al-Cu and Al-Ni, are some of the preferred alloys in the transportation industry, especially in the automotive industry, due to their strong corrosion behavior, high strength, and castability.

In recent years, new solidification control parameters such as ultrasonic vibration, selective laser melting, alternating current, direct current, and voltage have been used to improve the solidification structure [15,16]. By controlling these parameters during solidification, the microstructure and the mechanical and physical properties can be improved. Numerous studies have focused on the use of time-varying magnetic fields such as propagating magnetic fields [17,18] and pulsed magnetic fields [19,20] to improve the solidification structure and reported that they improved the solidification structure under magnetic fields [17,21–23]. Ma et al. [24] applied alternative electric fields to the BiMn/Bi eutectic alloy during directional solidification and examined the thermal and fluid effects it caused. As a result of the study, they reported that microstructure formation depends on the frequency of AC and changes spontaneously as an alternative electric field is applied. Liu et al. [25] presented the effects of applied positive and

* Corresponding author.
E-mail address: pinarata_88@hotmail.com (P.A. Esener).

https://doi.org/10.1016/j.tca.2024.179828
Received 6 June 2024; Received in revised form 16 July 2024; Accepted 17 July 2024
Available online 18 July 2024

negative electric fields on the directional solidification of Al-Cu eutectic alloy. Thus, they reported that applied positive and negative electric fields increased the grain size. Recently, Basit et al. [26,27] studied the solidification of Al-33 wt. % Cu and Al-6.4 wt. % Ni alloys, which are eutectic systems, by applying electric fields of different magnitudes parallel and opposite to the solid-liquid interface growth direction. In the study, the electric field size was (7–10) kV cm^{-1} and it was reported that the magnitude as well as the direction of the static electric field effectively affected the microstructure and mechanical properties of eutectic alloys. Another similar study is the article presented by Birinci et al. [28], in which the irregular microstructure and mechanical properties resulting from the solidification of the Al-12.6 wt. % Si alloy, which has an irregular eutectic structure, according to the electric field direction and magnitude, are examined. In the research, it was reported that since the silicon element is a semiconductor, the direction and magnitude of the applied electric field do not affect the irregularity of the Si phase and do not have much effect on the microstructure and mechanical properties. It was also reported in Reference [26–28] that the applied static electric field affected the mass transfer during solidification. The phenomenon of production in space (partial gravity or zero gravity) is becoming increasingly important for space research. Considered in this context, this new method and its effect on the properties of the material may have high potential for studies in this field.

In light of all this information, some efforts have been spent on the solidification of alloys under E_+ and E_-. To date, in the literature, a few studies on the solidification of the alloy under external static electrical fields have directions parallel or antiparallel to the growth direction of the solid-liquid interface [26-28] but no data has been presented regarding the effects of E_+ and E_- on the K and σ values for the alloys. This study aims to examine the effects of E_+ and E_- on the K and σ for Al−33 wt. % Cu, Al−6.4 wt. % Ni and Al−12.6 wt. % Si eutectic alloys solidified.

2. Experimental process

2.1. Experimental setup for the growth of eutectic structure with static electrical field

To investigate only the effect of the static electric field on solidification, it is necessary to set up a specialized apparatus that is free from any possible current or pulse. A new experimental setup for the solidification of binary or multi-component alloys in a uniform static electric field has been developed by Basit et al. [26]. The details of this mechanism used in the present work for the growth of Al-Cu, Al-Ni, and Al-Si eutectic structures under a static electric field are given in the literature [26]. The system consists of a preheating solidification furnace, an external static electric field system, and a cooling tank (Fig. 1).

The alloy to be solidified directionally under a static electric field should not solidify until the static electric field is fed into the system and becomes stable. Therefore, the preheated furnace (solidification furnace) used in the system maintains the molten alloy, which is carried from the vacuum melting furnace, above its melting point. This ensures that the samples solidify completely under the electric field. A K-type thermocouple positioned in the center of the heating zone was used by an on/off temperature controller to regulate the furnace's temperature.

The system includes a cooling tank that enables linear solidification. The tank is integrated in a way that allows a portion of it to enter the preheated furnace. The temperature of the cooling fluid circulated in the cooling tank is set at 291 K using a heating/refrigerating circulating bath.

A static electrical field circuit line is put up to apply strong static electrical fields to molten alloy. To set up this line, the DC high voltage

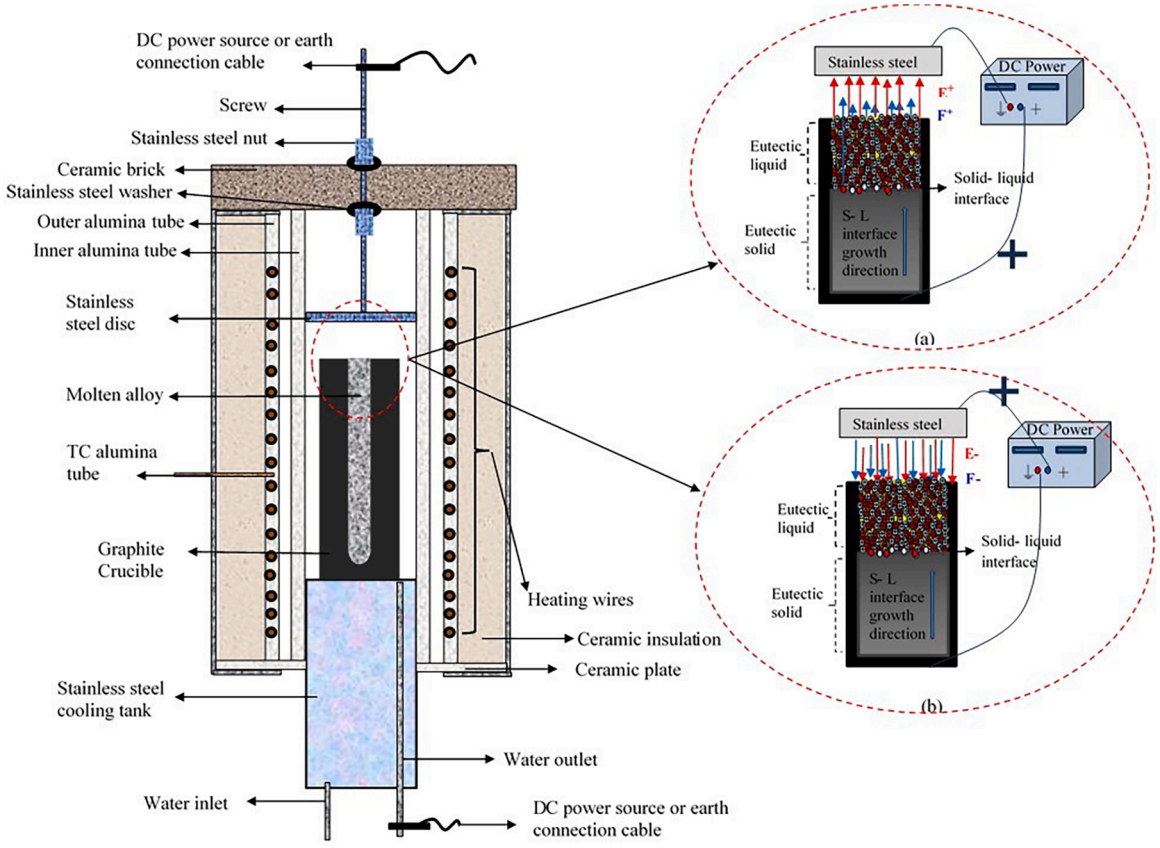

Fig. 1. Experimental setup for directional solidification with a static electrical field and Schematic illustration of the growth under the static electrical field at different directions (a) positive and (b) negative.

power supply is directly connected to the graphite specimen pot, and a metal disc spaced at the top of the specimen pot is connected earth or vice versa. A DC high voltage power supply of the FUG HCP 1400–35,000 type provided from Germany is used to generate a high static electrical field. This device has an adjustable high voltage (35 kV) and low current (maximum 40 mA) output for a high electric field.

The distance between the top of the specimen pot and the stainless steel disc was adjusted to approximately 5–8 mm according to the experimental conditions. A space maker was used to measure the distance with great sensitivity between the top of the specimen pot and the stainless steel disc. The measured value of ΔX and the applied voltage were used to determine the electrical field on the specimen. The measurements of the distance between the stainless steel disk and the top of the specimen pot have an estimated error of 2.7 % [26].

2.2. Electrogrowth of the eutectic alloys (Al-wt. %33 Cu, Al-6.4 wt. % Ni, and Al-12.6 wt. % Si) with the static electrical field

In the current study, 4 N purity Al and at least 3 N purity Cu, Ni, and Si elements supplied from Alfa Aesar company were used to prepare Al eutectic alloys (Al-wt. %33Cu, Al-6.4 wt. %Ni, and Al-12.6 wt. %Si). After melting in a graphite pot under a vacuum with a sufficient amount of weighted elements, the molten alloys are mixed at least five times to get homogenized with a graphite rod. Meanwhile, the electric field solidification furnace temperature was set above the eutectic melting point of each alloy to be prepared and kept constant there. These values are approximately 821.3 K, 915 K, and 850 K for Al-Cu, Al-Ni, and Al-Si eutectics, respectively [29]. Following the homogenization of the molten alloy, the graphite crucible containing the molten alloy was positioned on the cooling tank and inserted into the solidification furnace. Before beginning solidification, a positive static electric field (E_+) or a negative static electric field (E_-) was applied to the molten alloy by connecting the power supply output probe to the cooling tank and then connecting the stainless steel disc spaced with the top of the graphite pot to the ground, or vice versa. The minimum electric field required to be applied to the molten alloy must be determined as it depends on the type of alloy. The amount of the electric field force that would affect the liquid ion atoms should be bigger than the total of the liquid atoms' frictional and tensional forces. Previous studies have determined the required minimum value for Al-based binary alloys to be 6 kV cm^{-1} [26].

After applying the required electric field to the liquid alloy, the cooling fluid is switched on and the input power to the heating furnace is switched off to solidify the molten alloy from bottom to top under the static electric field. To guarantee complete solidification of the alloys under the electric field, the DC power supply input is switched off when the temperature of the solidification furnace falls 50 K below the alloy's melting temperature.

Finally, the solidified specimen was removed from the graphite pot and then was rapidly quenched with cool water (298 K). Solidification experiments were carried out with electric fields of varying magnitudes, in positive and negative directions, depending on the compositions. These magnitudes are (+10) and (-10) kV cm^{-1} for Al-Cu and Al-Ni eutectic, and (+16) and (-16) kV cm^{-1} for Al-Si eutectic in different directions. Furthermore, an additional sample as a reference sample was solidified for each composition without the application of an electric field, using the same solidification conditions. The total experimental error in determining E was calculated as 3.0 % [26]. To avoid experimental errors caused by different solidification conditions, the current solidification conditions, such as heating oven temperature, melting temperature, cooling liquid temperature, sample diameter, and liquid flow rate were determined and kept constant for directional solidification experiments with high static electric fields.

2.3. Microstructures of Al-Cu, Al-Ni, and Al-Si eutectic alloys solidified with the external static electrical field

The microstructure images of Al-Cu, Al-Ni, and Al-Si eutectic alloys solidified with the static electrical fields were taken from cross-sections of samples using a *Nikon ECLIPSE MA100* model optical reverse metal microscope. Typical optical images of Al-Cu, Al-Ni, and Al-Si eutectic alloys solidified under none electrical field and different directions and magnitudes of static high electric field are shown in Fig. 2.

The influences of direction and magnitude of external stoical electrical field on microstructures, eutectic spacing, grain sizes, and mechanical properties in the Al-Cu, Al-Ni, and Al-Si eutectic alloys were extensively investigated in References [26,27,28]. In the present work, the influences of external static electrical fields on thermal and electrical conductivity are aimed. As can be seen from Fig. 2 the positive electrical fields increase the eutectic spacing while the negative electrical fields decrease the eutectic spacing. Thus, the positive static electrical field increases thermal and electrical conductivity while the negative static electrical field should decrease thermal and electrical conductivity.

2.4. Thermal conductivity measurements

There are many different methods to determine the thermal conductivity of solid materials. The longitudinal heat flow system is a system designed to measure the change in thermal conductivity of solid materials with temperatures up to 900 °C.

The longitudinal heat flow system consists of two systems: a heater and a cooler (Fig. 3). The heating system consists of a cylindrical heater and a copper block fixed inside. The cylindrical heater consists of a 100 mm long hot zone created by winding a resistance wire insulated with ceramic beads on an alumina tube with dimensions of 80 mm ODx60 mm IDx150 mm. To control the temperature of the heating area, a thermocouple is placed at the middle point of the heating area and on the ceramic bead, and a temperature controller is connected. The temperature of the heating system was controlled to an accuracy of ± 0.01°C with a Eurotherm 2604-type temperature controller. The cylindrical cooling system consists of a stainless steel pipe with dimensions of 60 mm ODx50 mm IDx150 mm, closed at one end. The other end is closed with a steel cap that has a screw holder with a diameter of 20 mm and a height of 5 mm at its middle point. There is a screw-on sample holder in the middle of the cover to hold/fix the sample in the vertical direction and to immerse the sample in the cooling liquid. There are connection pipes for the inlet and outlet of the coolant. In addition, the outlet ends of the thermocouples to be placed in the sample are placed through 10 mm diameter holes at the middle point and side surface of the cooler. Cooling was achieved using a PolyScience heating/cooling circulation bath containing an aqueous ethylene glycol solution. The temperature of the circulating bath was kept constant at 0°C. The sample, solidified under a static electric field of different directions and sizes, is removed from the graphite crucible and placed in the longitudinal heat flow system to measure heat conduction.

To determine the power transferred to the system when the system is stable, set to the desired temperature by the temperature controller, the current passing through the heater and the potential drop are determined with SIGLENT SDM3055 model multimeters. K-type three thermocouples were used to measure the thermal conductivity coefficient of the solid phase. These thermocouples are placed inside the sample at 3–4 mm intervals. The temperature values read at the point where each thermocouple is located are recorded by transferring them to the computer with the Pico TC-08 model data logger.

The sample is heated from one end to the desired temperature by powering to the temperature system, while the other end is kept in the cooling system. Thus, a constant temperature gradient is created longitudinally on the sample. In the longitudinal heat flow system, in equilibrium, the thermal conductivity is expressed by Eq. (1) from the Fourier-Biot law [30–32].

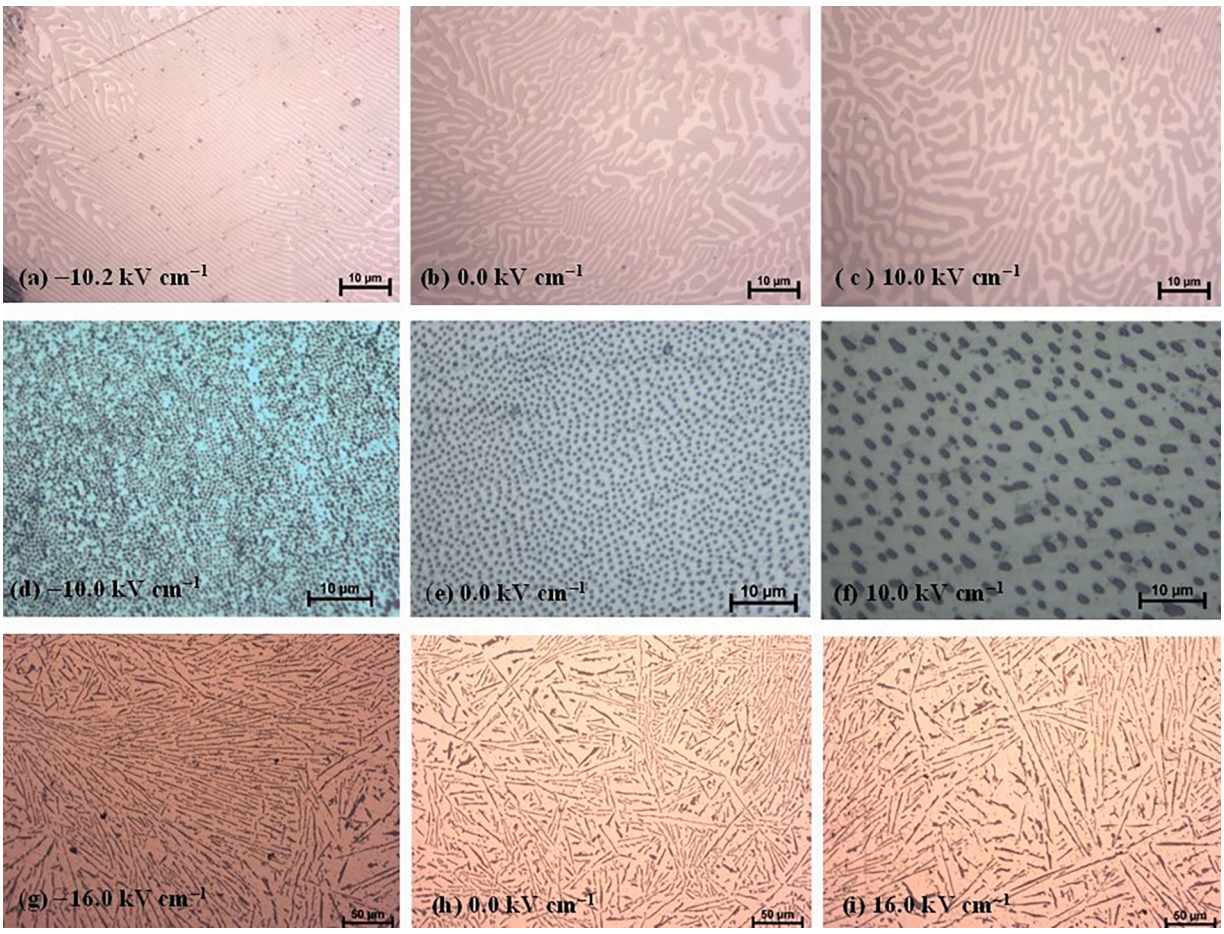

Fig. 2. Typical microstructure optical images of the eutectic alloys solidified under different magnitudes and directions of electric field; (a), (b), and (c) for the Al-Cu , (d), (e) and (f) for the Al-Ni and (g), (h) and (i) for the Al-Si.

$$K = -\frac{Q\Delta X}{A\Delta T} \tag{1}$$

Here, K is the thermal conductivity, Q is the heat flow rate, A is the surface area perpendicular to the heat flow, that is, the cross-section of the sample, $\Delta T=T_2-T_1$ is the temperature difference of the thermocouples in the sample, and $\Delta X=X_2-X_1$ is the distance between the thermocouples.

For thermal conductivity measurements, first of all, liquid Al-33 wt. % Cu, Al-6.4 wt. % Ni and Al−12 wt. % Si eutectic alloys were formed in a vacuum melting furnace in a 20 mm diameter graphite crucible [33, 34]. Then, molten alloys in a 20 mm diameter graphite crucible were solidified under three different conditions: first of them is without statical electrical field, second of them is under positive statical electrical field and third of them is under negative statical electrical field.

The samples were heated in 50 K steps to approximately 250−350 K temperature until they stabilized for approximately one hour at each temperature step. The accuracy of thermal conductivity measurement in the longitudinal heat flow method is more precisely dependent on the measurement of the heat flow rate through to sample. A comparison method was used to get right the measurement of the heat flow rate through to the sample. The thermal conductivity of pure aluminium is well known in the literature. A reference sample from pure aluminium was prepared and the aluminium pure sample was then heated in the 50 °C steps up to 650 °C which is roughly 15 °C below the melting point of pure aluminium. The required heat flow rate through to pure aluminium sample was determined from the Fourier-Biot law for each steady state conduction. The Fourier-Biot law for pure aluminium sample is written as

$$Q_{required} = -K_{pureAl}A\frac{\Delta T}{\Delta X} \tag{2}$$

where $Q_{reqired}$ is the required input power to increase the sample temperature for each steady state, $K_{pure\ Al}$ is the thermal conductivity of pure aluminum reference sample at each steady state which is known in the literature. Therefore, for each steady state, "input power correction coefficient (α)" is required to get an accurate K value. The value of α for each steady state is normally smaller than one and can be expressed as

$$\alpha = \frac{Q_{required}}{Q_{input}} \tag{3}$$

where Q_{input} is the input power given to the longitudinal heat flow apparatus to increase the temperature of the pure aluminium sample to steady state condition. In this case, by replacing the $Q = \alpha\, Q_{input}$ into Eq. (1), the thermal conductivity for any kind of sample at steady state condition is expressed with Eq. (4).

$$K = -\alpha Q_{input}\frac{1}{A}\frac{\Delta X}{\Delta T} \tag{4}$$

Experimental data regarding the measured force compliance coefficient for pure aluminum are given in Table 1.

In the longitudinal heat flow system, there are uncertainties in the experimental parameters. The total uncertainty is about 9 %, which is about 4.4 % from the current measurement; the estimated error in the potential drop measurement is about 0.6 %, about 2.5 % from the measurement of temperature differences, about 0.5 % from the thermal conductivity measurement, and about 0.7 % from the cross-sectional

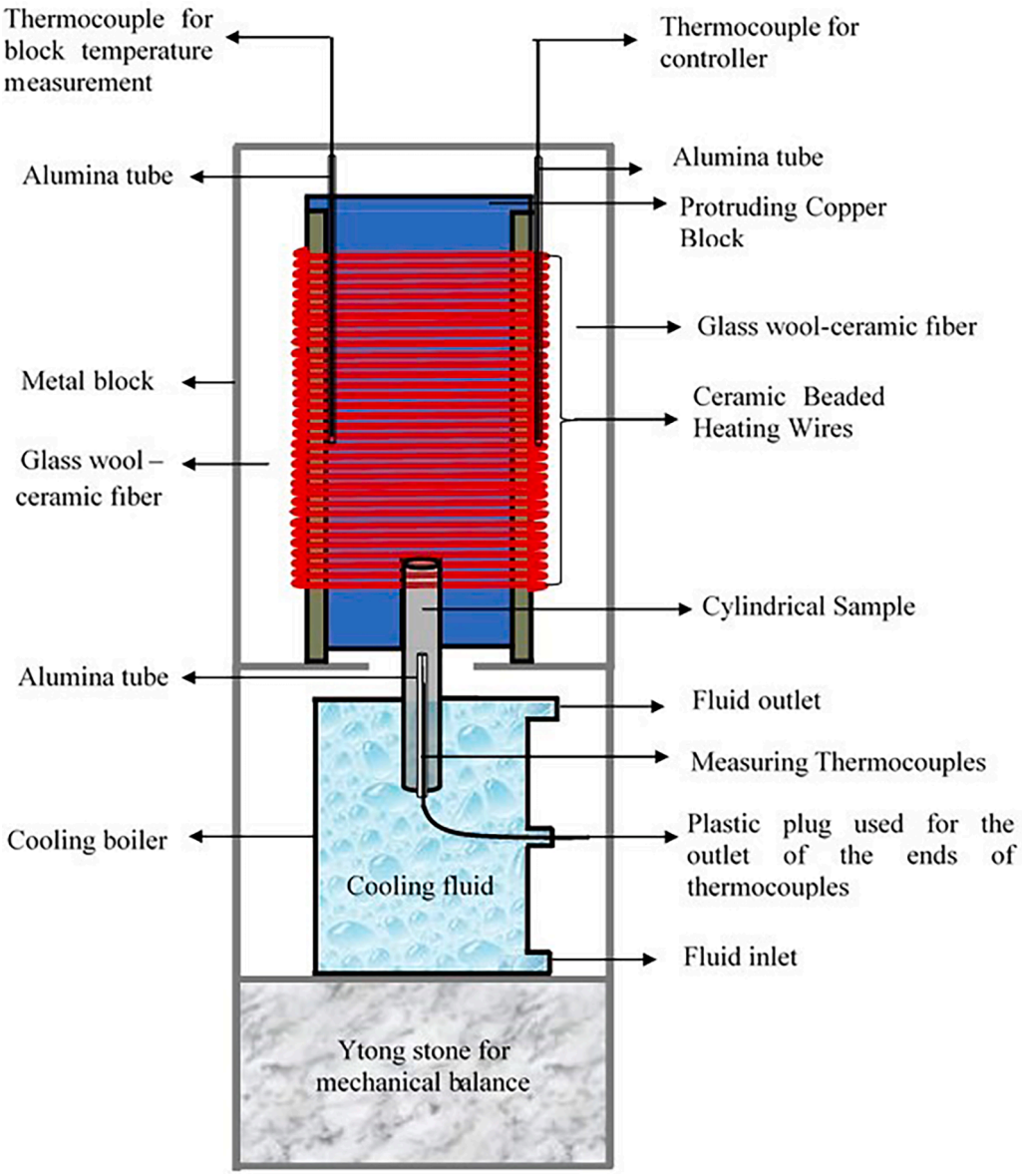

Fig. 3. Block diagram of longitudinal heat flow apparatus used for measuring thermal conductivity.

Table 1
Power compatibility coefficients of pure aluminum at different steady-state temperatures using the thermal conductivity in the literature as reference.

Steady-State Temperature, T (K)	Block Temperature, T (K)	References Thermal Conductivity, K_R (W/mK)	Temperature Difference, ΔT (K)	Distance, ΔX (m)	Input power, Q_{input} (W)	Required power, $Q_{necessary}$ (W)	Coefficient, α
313	310	248.9	0.385	0.0034	6.34322	8.60379763	1.35637699
373	365.90	245.6	0.853	0.0034	24.1898	18.8097037	0.77758823
423	414.30	242.8	1.000	0.0034	33.9031	21.7998368	0.64300423
473	461.80	239.9	1.286	0.0034	48.2126	27.6997454	0.57453333
523	508.90	237.3	1.608	0.0034	64.9054	34.2600777	0.52784634
573	655.80	234.4	2.295	0.0034	90.3715	48.2997473	0.53445774
623	599	231.6	2.959	0.0034	119.786	61.5301652	0.51366913
673	647	229.0	3.181	0.0034	135.612	65.40391	0.48228562
723	692.60	226.1	3.747	0.0034	161.864	76.0656913	0.46993611
773	738	223.6	4.350	0.0034	189.128	87.3304337	0.46175209
823	778	221.0	4.616	0.0034	209.847	91.593074	0.43647508
873	822.70	218.1	5.496	0.0034	244.773	107.62346	0.43968771
923	868	215.6	6.127	0.0034	271.228	118.604508	0.43728743
973	915.60	212.9	5.770	0.0034	299.475	110.295053	0.36829469

area and constant distance measurement [35].

With the longitudinal heat flow system, the thermal conductivity of each sample was determined by measuring the voltage, current transferred to the system, and the temperature of the sample at steady state temperatures.

2.5. Electrical conductivity measurements

A current source and potential drop are needed to determine electrical resistivity/conductivity, which is one of the characteristic properties of materials. The electrical resistivity (ρ) of a material is found by the ratio of current (I) and voltage (V) flowing through the sample (Eq. (5)).

$$\rho = \frac{V}{I} G \tag{5}$$

In case it becomes necessary to use the four-point conductivity measurement technique to determine the resistivity of the sample, it is necessary to reveal the contribution of the G (Geometric Correction Coefficient/Factor) value of the sample to the resistivity. Detailed information about the Geometric Correction Coefficient/ Factor is given in Reference [36].

The change in electrical resistivity/conductivity values of the alloys with temperature was determined by the four-point conductivity measurement method shown in Fig. 4. As seen in Fig. 4, four probes contact the sample. These wires have a circular cross-section and are made of platinum. The two wires in the middle are the potential difference (V), and the wires on the outer edge are the contact points that measure current (I). The distances between the probes are equal to each other and set at 1 mm. Determining the thickness of the samples and the distance between the probes affects the value of the G factor. The apparatus in which the experiment was carried out includes a *Protherm* brand muffle furnace working with a PC442T controller and a measuring instrument for measuring current and potential differences. There is a 0.5 mm K-type thermal couple inside the oven to measure the temperature of the oven during the experiment. The current, potential difference, and temperature obtained from the sample whose conductivity will be measured are recorded on the computer with the help of a program. The error in the electrical resistivity measurements is calculated at about 5 %.

The changes in the electrical resistivity/conductivity of the alloys with temperature were determined by cutting 2.5–3.5 mm lengths from 10 mm diameter and 80 mm long cylindrical samples solidified under static electric fields of different directions and sizes.

3. Results and Discussion

3.1. Influences of E_+ and E_- on the K

The variation of thermal conductivity of the Al-Cu, Al-Ni, and Al-Si eutectic alloys solidified with different values of E_+ and E_- are shown in Fig. 5. It is seen that the thermal conductivity decreases with increasing temperature in Fig. 5(a), Fig. 5(b) and Fig. 5(c). Heat conduction in metals is provided by electrons and phonons. However, increasing the temperature will increase the lattice distortion and therefore increase the scattering of electrons and phonons. Thus, the mean free path of electrons and phonons decreases and the thermal conductivity decreases [37,38].

In Fig. 5(a), the thermal conductivity value of the Al-33Cu eutectic alloy solidified with none electric field was measured as 174.16 W/m K for 313 K temperature. The thermal conductivity value of Al-33Cu casting alloy at 313 K temperature reported by Aksöz et al. [39] was reported to be approximately 127 W/m K. The thermal conductivity value of Al-33Cu eutectic alloy at 313 K temperature was measured as 183.85 W/m K when solidified under a (+10) kV cm^{-1} positive electric field, and 167.84 W/m K when solidified under a (-10.2) kV cm^{-1} negative electric field. In Fig. 5(b), the thermal conductivity value of Al-6.4Ni eutectic alloy solidified with none electric field is 245.43 W/m K at 313 K temperature. The thermal conductivity of Al-4.7Ni casting alloy reported by Manuel et al. [40] was reported as 111 W/m K at 298

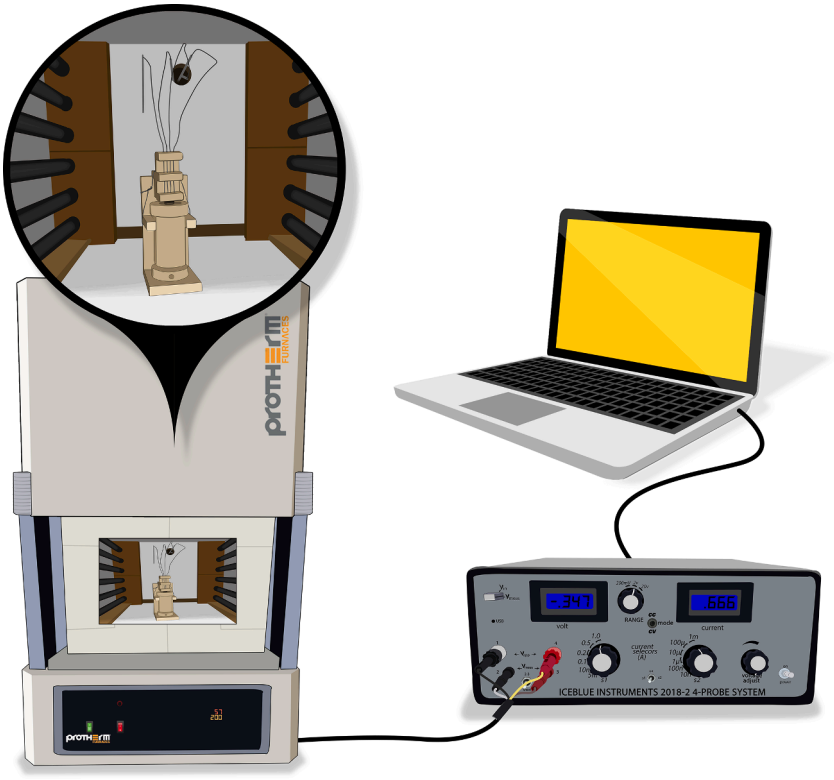

Fig. 4. The schematic diagram of the four-point probe method used for measuring electrical resistivity/conductivity.

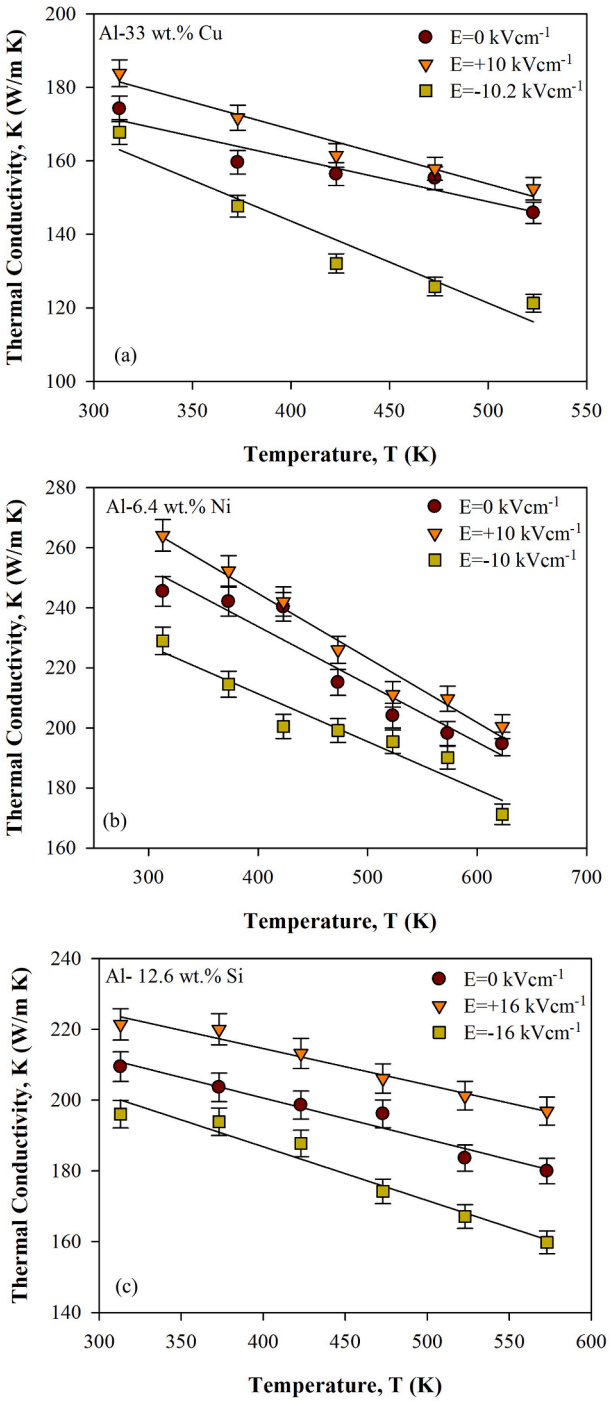

Fig. 5. Thermal conductivity variations with the temperature and magnitudes of the static electrical field in the (a) Al-Cu, (b) Al-Ni, and (c) Al-Si eutectic alloys.

K. In this study, by solidifying the Al-6.4Ni eutectic alloy under a (+10) kV cm^{-1} positive electric field, the thermal conductivity value at 313 K temperature was measured as 264.10 W/m K, while by solidifying it under a (-10) kV cm^{-1} negative electric field, the thermal conductivity value at 313 K temperature was found to be 228.94 W/m K. In Fig. 5(c), the thermal conductivity value of Al-12Si eutectic alloy solidified with none electric field was measured as 209.42 W/m K for 313 K temperature. The thermal conductivity of the Al-13Si casting alloy reported by Zhang and Li [41] was reported as 121 W/m K at 298 K temperature. By solidifying the Al-12Si eutectic alloy under a (+16) kV cm^{-1} positive electric field, the thermal conductivity value at 313 K temperature was measured as 221.38 W/m K, while by solidifying it under a (-16) kV cm^{-1} negative electric field, it was measured as 196.03 W/m K. As seen from the thermal conductivity-temperature curves in Fig. 5(a), Fig. 5(b), and Fig. 5(c), the thermal conductivity of the alloys solidified under a positive electric field increased, while the thermal conductivity of the alloys solidified under a negative electric field showed a decreasing effect. In previous studies, microstructural changes resulting from the solidification of Al-Cu, Al-Ni, and Al-Si eutectic alloys under positive and negative electric fields have been reported in detail [26–28]. The parallel and antiparallel electric field applied to the solid-liquid interface of the alloys creates an electrical force on the liquid atoms or molecules. This leads to an increase or decrease in the number of atoms or molecules passing from the liquid phase to the solid phase. It has been reported that E_+ and E. applied in Reference [26–28] decreased or increased microstructure parameters such as lamellar spacing, grain size, and some mechanical properties. The change in thermal conductivity with the applied electric field is also directly related to the change in the microstructure. In the samples solidified under a positive electric field, it was observed that the phases in the microstructure expanded, thus the grain growth increased and the number of grains decreased. As a result, the reduction of grain boundaries in the microstructure increases the thermal conductivity as it increases the free path that electrons and phonons can take. Similarly, it has been reported that in samples solidified under a negative electric field, the phases in the microstructure become thinner, the grain size decreases, and the number of grains increases [26–28]. Increases in grain boundaries in the microstructure reduce the free path of electrons and phonons, causing a decrease in thermal conductivity.

3.2. *Influences of E_+ and E_- on the σ*

The variation of electrical conductivity of the Al-Cu, Al-Ni, and Al-Si eutectic alloys solidified with different values of E_+ and E_- are shown in Fig. 6. It is seen that the electrical conductivity decreases with increasing temperature in Fig. 6(a), (b) and (c). Defects (dislocations) formed by atoms in the crystal structure cause thermal and electrical conductivity to decrease with increasing temperature. However, factors such as impurities, heating, deformation, grain size, and chemical composition also affect electrical conductivity [36].

In Fig. 6(a), the electrical conductivity value of the Al-33Cu eutectic alloy solidified with none electric field was measured as 0.020 ($\times 10^8$)/Ωm for 323 K. The electrical conductivity value of Al-33Cu eutectic alloy at 323 K temperature was measured as 0.0311 ($\times 10^8$)/Ωm under a (+10) kV cm^{-1} positive electric field, while it was measured as 0.0164 ($\times 10^8$)/Ωm under a (-10.2) kV cm^{-1} negative electric field. In Fig. 6(b), the electrical conductivity value of the Al-6.4Ni eutectic alloy solidified with none electric field was determined as 0.0298 ($\times 10^8$)/Ωm for 323 K temperature. The electrical conductivity of the Al-6Ni casting alloy reported by Muriana et al. [42] was reported to be 0.048 ($\times 10^8$)/Ωm at room temperature. The electrical conductivity value of the Al-6.4Ni eutectic alloy at 323 K temperature was measured as 0.0423 ($\times 10^8$)/Ωm when solidified under a (+10) kV cm^{-1} positive electric field, while it was measured as 0.0139 ($\times 10^8$)/Ωm when solidified under a (-10) kV cm^{-1} negative electric field. In Fig. 6(c), the electrical conductivity value of the Al-12Si eutectic alloy solidified with none electric field was measured as 0.0286 ($\times 10^8$)/Ωm at 323 K temperature. Brandt and Neuer [43] reported the electrical conductivity of Al-12Si casting alloy as 0.0235 ($\times 10^8$)/Ωm at room temperature. By solidifying the Al-12Si eutectic alloy under a (+16) kV cm^{-1} positive electric field, the electrical conductivity value at 323 K temperature was measured as 0.0325 ($\times 10^8$)/Ωm, while by solidifying it under a (-16) kV cm^{-1} negative electric field, this value was measured as 0.00291 ($\times 10^8$)/Ωm. As seen in Fig. 6(a), (b), and (c), the electrical conductivity of the alloys solidified under a positive electric field increased, while the electrical conductivity of the alloys solidified under a negative electric field showed a decreasing effect. Changes in the microstructure

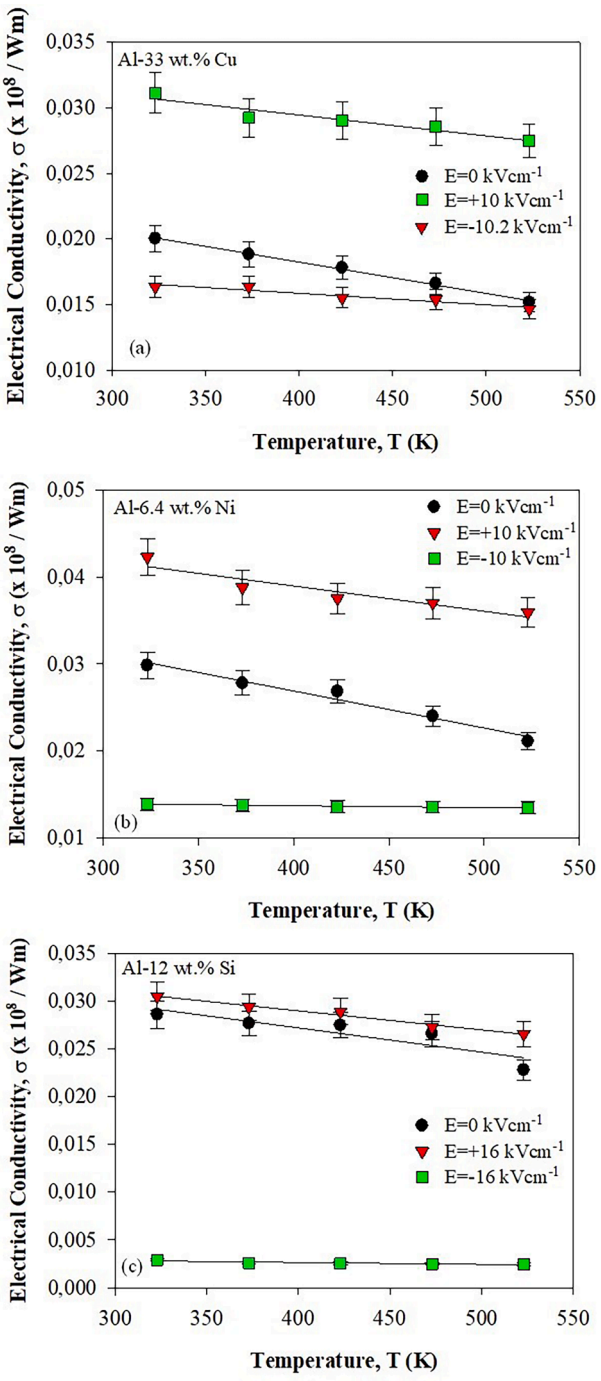

Fig. 6. Electrical conductivity variations with the temperature and magnitudes of the static electrical field in the (a) Al-Cu, (b) Al-Ni, and (c) Al-Si eutectic alloys.

depending on the direction and magnitude of the applied electric field caused changes in electrical conductivity as well as thermal conductivity. In samples solidified under a positive electric field, electrical conductivity increased with the decrease in the number of grains in the microstructure, and electrical conductivity decreased with the increase in the number of grains under a negative electric field.

Influences of Directions and Magnitudes of Static Electrical Field on Microstructure and Mechanical Properties in the Al-Si Eutectic Alloy were studied by Birinci et. al [28]. According to their conclusion "The liquid Si atom was not charged as Si^{+4e} cation because of Si only occurs as ions on the gas phase and only at very high temperatures in a vacuum or inert gas. Therefore, when E_+ and E_- are applied into the Al-Si molten alloy, the liquid Al atom was only charged as Al^{+3e} cation by E_+ and E_- and thus, the F_+ and F_- affect Al^{+3e} cations and do not affect the uncharged Si atom. The mass transfer of liquid Al atom is affected by F_+ and F_- and the mass transfer of liquid Si atom is not affected by F_+ and F_- during the solidification of Al-Si molten eutectic alloy under static electrical field. Therefore, the thickness of Al_α phase is expanding by increasing the value of E_+ or getting thinner by increasing the value of E_-. However, the thickness of Si phase was not considerably changed with increasing the values of E_+ and E_- [28]". Therefore, the eutectic spacing in the Al-Si just increases or decreases due to widening or thinning of Al_α phase with E_+ and E_-, respectively. Thus thermal and electrical conductivity of Al-Si eutectic alloy solidified E_+ and E_- are higher or smaller than thermal and electrical conductivity of Al-Si eutectic alloy solidified with none static electrical field.

4. Conclusions

The changes in thermal conductivity and electrical conductivity with temperature for the Al-Cu, Al-Ni, and Al-Si eutectic alloys solidified under none, positive, and negative static electric fields were measured by the longitudinal heat flow method and the four-point probe method, respectively. The important points obtained from the current results of thermal and electrical conductivity analyses are listed in bullet points.

1. Thermal and electrical conductivity values for the Al-Cu, Al-Ni, and Al-Si eutectic alloys solidified under none, E_+, and E_- decrease linearly with increasing temperature.
2. The applied positive and negative electric field creates an electric force at the solid-liquid interface. The resulting electrical force causes a time-dependent increase or decrease in the transition of atoms or molecules from liquid to solid. This has led to changes in the microstructure and hence in the K and σ values of alloys. Thus, while the E_+ increased the values of K and σ, the E_- decreased their values in the Al-33 wt. % Cu, Al-6.4 wt. % Ni and Al-12 wt. % Si as expected the changes of mechanical properties.
3. By applying different magnitudes of electric fields to Al-Cu, Al-Ni, and Al-Si eutectic alloys in different directions, the dependence of K and σ on the E_+ and E_- can be examined and thus the current study can be expanded.
4. From experimental results, it can be concluded that the electric field direction and magnitude may offer an additional solidification control parameter according to the desired physical properties of the alloy to be produced.

CRediT authorship contribution statement

Sercan Basit: Writing – review & editing, Writing – original draft, Visualization, Validation, Supervision, Methodology, Investigation, Formal analysis, Data curation. **Pınar Ata Esener:** Writing – review & editing, Writing – original draft, Visualization, Validation, Investigation, Data curation. **Yiğit Yavuz Aydoğan:** Writing – review & editing, Writing – original draft, Visualization, Validation, Supervision, Investigation, Data curation. **Sezen Aksöz:** Writing – review & editing, Writing – original draft, Visualization, Validation, Methodology, Investigation, Data curation. **Necmettin Maraşlı:** Writing – review & editing, Writing – original draft, Visualization, Validation, Project administration, Methodology, Investigation, Funding acquisition, Data curation.

Declaration of competing interest

The authors declare that they have no known competing financial interests or personal relationships that could have appeared to influence the work reported in this paper.

Data availability

The authors do not have permission to share data.

Acknowledgments

This research was supported financially by the Scientific and Technical Research Council of Turkey (TÜBİTAK) under contract no. 118M695. The authors are grateful to the Scientific and Technical Research Council of Turkey (TÜBİTAK) for their financial support.

References

[1] I. Minkoff, Solidification/liquid state processes. Materials Processes, Springer, Berlin Heidelberg, 1992, pp. 1–31, https://doi.org/10.1007/978-3-642-95562-4_1.
[2] W. Kurz, D.J. Fisher, Fundamentals of solidification, 3rd edn., Aedermannsdorf, Switzerland, 1989.
[3] J. Lapin, Z. Gabalcová, Solidification behaviour of TiAl-based alloys studied by directional solidification technique, Intermetallics. (Barking) 19 (6) (2011) 797–804, https://doi.org/10.1016/j.intermet.2010.11.021.
[4] R. Reviere, G. Sauthoff, D.R. Johnson, B.F. Oliver, Microstructure of directionally solidified eutectic based Fe(Al, Ta)/Fe_2Ta(Al) alloys as a function of processing conditions, Intermetallics. (Barking) 5 (3) (1997) 161–172, https://doi.org/10.1016/S0966-9795(96)00081-7.
[5] S. Zhao, J. Li, L. Liu, Y. Zhou, Eutectic growth from cellular to dendritic form in the undercooled Ag-Cu eutectic alloy melt, J. Cryst. Growth 311 (5) (2009) 1387–1391, https://doi.org/10.1016/j.jcrysgro.2008.12.006.
[6] R. Kakitani, R.V. Reyes, A. Garcia, J.E. Spinelli, N. Cheung, Relationship between spacing of eutectic colonies and tensile properties of transient directionally solidified Al-Ni eutectic alloy, J. Alloys. Compd. 733 (2018) 59–68, https://doi.org/10.1016/j.jallcom.2017.10.288.
[7] R.J. Vikram, S.A. Gokulnath, K.G. Prashanth, S. Suwas, Effect of scanning strategy on microstructure and texture evolution in a selective laser melted Al-33Cu eutectic alloy, J. Alloys. Compd. 936 (2023) 168098, https://doi.org/10.1016/j.jallcom.2022.168098.
[8] S. Amirkhanlou, S. Ji, A review on high stiffness aluminum-based composites and bimetallics, Crit. Rev. Solid State Mater. Sci. 45 (2020) 1–21, https://doi.org/10.1080/10408436.2018.1485550.
[9] A. Inoue, Amorphous, nanoquasicrystalline and nanocrystalline alloys in Al-based systems, Prog. Mater. Sci. 43 (1998) 365–520, https://doi.org/10.1016/S0079-6425(98)00005-X.
[10] W. Haupin, Aluminum, Encyclopedia of Physical Science and Technology, Elsevier, 2003, pp. 495–518. Third edition.
[11] C.S. Tiwary, P. Pandey, S. Sarkar, R. Das, S. Samal, K. Biswas, K. Chattopadhyay, Five decades of research on the development of eutectic as engineering materials, Prog. Mater. Sci. 123 (2022) 100793, https://doi.org/10.1016/j.pmatsci.2021.100793.
[12] S.J. Wang, G. Liu, J. Wang, A. Misra, Characteristic orientation relationships in nanoscale Al-Al_2Cu Eutectic, Mater. Charact. 142 (2018) 170–178, https://doi.org/10.1016/j.matchar.2018.05.037.
[13] H. Kaya, U. Böyük, E. Çadırlı, N. Maraşlı, Measurements of the microhardness, electrical and thermal properties of the Al-Ni eutectic alloy, Mater. Des. 34 (2012) 707–712, https://doi.org/10.1016/j.matdes.2011.05.030.
[14] C. Suwanpreecha, P. Pandee, U. Patakham, C. Limmanevichitr, New generation of eutectic Al-Ni casting alloys for elevated temperature services, Mater. Sci. Eng. 709 (2018) 46–54, https://doi.org/10.1016/j.msea.2017.10.034.
[15] E. Sjölander, S. Seifeddine, The heat treatment of Al-Si-Cu-Mg casting alloys, J. Mater. Process. Technol. 210 (2010) 1249–1259, https://doi.org/10.1016/j.jmatprotec.2010.03.020.
[16] S. Hegde, K.N. Prabhu, Modification of eutectic silicon in Al-Si alloys, J. Mater. Sci. 43 (2008) 3009–3027, https://doi.org/10.1007/s10853-008-2505-5.
[17] J.C. Jie, S.P. Yue, J. Liu, D.H. StJohn, Y.B. Zhang, E.Y. Guo, T.M. Wang, T.J. Li, Revealing the mechanisms for the nucleation and formation of equiaxed grains in commercial purity aluminum by fluid-solid coupling induced by a pulsed magnetic field, Acta Mater. 208 (2021) 116747, https://doi.org/10.1016/j.actamat.2021.116747.
[18] Y.K. Zhang, J. Gao, D. Nagamatsu, T. Fukuda, H. Yasuda, M. Kolbe, J.C. He, Reduced droplet coarsening in electromagnetically levitated and phase-separated Cu-Co alloys by imposition of a static magnetic field, Scr. Mater. 59 (9) (2008) 1002–1005, https://doi.org/10.1016/j.scriptamat.2008.07.005.
[19] T. Liu, Q. Wang, A. Gao, C. Zhang, C. Wang, J. He, Fabrication of functionally graded materials by a semi-solid forming process under magnetic field gradients, Scr. Mater. 57 (2007) 992–995, https://doi.org/10.1016/j.scriptamat.2007.08.011.
[20] M. Dong, T. Liu, J. Liao, Y. Xiao, Y. Yuan, Q. Wang, In situ preparation of symmetrically graded microstructures by solidification in high-gradient magnetic field after melt and partial-melt processes, J. Alloys. Compd. 689 (25) (2016) 1020–1027, https://doi.org/10.1016/j.jallcom.2016.08.074.
[21] V. Metan, K. Eigenfeld, D. Räbiger, M. Leonhard, S. Eckert, Grain size control in Al-Si alloys by grain refinement and electromagnetic stirring, J. Alloys. Compd. 487 (2009) 163–172, https://doi.org/10.1016/j.jallcom.2009.08.032.
[22] Y.H. Zhang, X.R. Cheng, H.G. Zhong, Z.S. Xu, L.J Li, Y.Y. Gong, X.C. Miao, C. J. Song, Q.J. Zhai, Comparative study on the grain refinement of al-si alloy solidified under the impact of pulsed electric current and travelling magnetic field, Metals. (Basel) 6 (7) (2016) 170, https://doi.org/10.3390/met6070170.
[23] Q.S. Li, C.J. Song, H.B. Li, Q.J. Zhai, Effect of pulsed magnetic field on microstructure of 1Cr18Ni9Ti austenitic stainless steel, Mater. Sci. Eng. A 466 (2007) 101–105, https://doi.org/10.1016/j.msea.2007.03.061.
[24] Y. Ma, L.L. Zheng, D.J. Larson, Microstructure formation during BiMn/Bi eutectic growth with applied alternating electric fields, J. Cryst. Growth 62 (2004) 620–630, https://doi.org/10.1016/j.jcrysgro.2003.10.018.
[25] B. Liu, Z. Zhao, Y. Wang, Z. Chen, The solidification of Al-Cu binary eutectic alloy with electric fields, J. Cryst. Growth 271 (2004) 294–301, https://doi.org/10.1016/j.jcrysgro.2004.06.009.
[26] S. Basit, S. Birinci, N. Maraşlı, Mater. Charact. 161 (2020) 110157, https://doi.org/10.1016/j.matchar.2020.110157.
[27] S. Basit, S. Birinci, N. Maraşlı, Growth of rod Structure with static electrical field in the Al-Ni eutectic system, J. Mater. Sci. Mater. Electron. 31 (2020) 14055–14068, https://doi.org/10.1007/s10854-020-03960-0.
[28] S. Birinci, S. Basit, N. Maraşlı, Influences of directions and magnitudes of static electrical field on microstructure and mechanical properties for Al-Si eutectic alloy, J. Mater. Eng. Perform. 31 (6) (2022) 5070–5079, https://doi.org/10.1007/s11665-021-06564-9.
[29] H. Baker, in: ASM Handbook, Alloy Phase Diagrams, vol. 3, 1741, 1992.
[30] J. B. Biot Traitt de Physique, vol. 4, 669 (1816).
[31] J. B, Fourier The Analytical Theory of Heat Gaulhier-Villars, English translation by A. Freeman, Paris, 1822.
[32] Cambridge University Press 466 (1878); a new edition of the English translation Dover Publications, 1955. New York.
[33] E. Çadırlı, U. Böyük, H. Kaya, N. Maraşlı, K. Keşlioğlu, S. Akbulut, Y. Ocak, The effect of growth rate on microstructure and microindentation hardness in the In-Bi-Sn ternary alloy at low melting point, J. Alloy. Compd. 470 (2009) 150–156, https://doi.org/10.1016/j.jallcom.2008.02.056.
[34] H. Kaya, U. Böyük, E. Çadırlı, Y. Ocak, S. Akbulut, K. Keşlioğlu, N. Maraşlı, Dependency of microstructural parameters and microindentation hardness on the temperature gradient in the In-Bi-Sn ternary alloy with a low melting point, Met. Mater. Int. 14 (5) (2008) 575–582, https://doi.org/10.3365/met.mat.2008.10.575.
[35] S. Aksöz, E. Öztürk. N. Maraşlı, The measurement of thermal conductivity variation with temperature for solid materials, Measurement 46 (1) (2013) 161–170, https://doi.org/10.1016/j.measurement.2012.06.003.
[36] P. Ata Esener, B. Demirel, S. Aksoz, Effect of Sb and In additives on thermal and electrical properties of Sn-9Zn-4Bi alternative lead-free solder alloy, Mater. Chem. Phys. 296 (2023) 127223, https://doi.org/10.1016/j.matchemphys.2022.127223.
[37] P. Ma, Z.J. Wei, Y.D. Jia, Z.S. Yu, K.G. Prashanth, S.L. Yang, C.G. Li, L.X. Huang, J. Eckert, Mechanism of formation of fibrous eutectic Si and thermal conductivity of SiCp/Al-20Si composites solidified under high pressure, J. Alloys. Compd. 709 (2017) 329–336, https://doi.org/10.1016/j.jallcom.2017.03.162.
[38] Y.S. Touloukian, R.W. Powell, C.Y. Ho, P.G. Klemens, Thermal conductivity metallic elements and alloys, 1, 1970, pp. 4a–11a. New York-Washington.
[39] S. Aksöz, Y. Ocak, N. Maraşlı, E. Çadırlı, H. Kaya, U. Böyük, Dependency of the thermal and electrical conductivity on the temperature and composition of Cu in the Al based Al-Cu alloys, Exp. Therm. Fluid. Sci. 34 (2010) 1507–1516, https://doi.org/10.1016/j.expthermflusci.2010.07.015.
[40] M.V. Canté, J.E. Spinelli, I.L. Ferreira, N. Cheung, A. Garcia, Microstructural development in Al-Ni alloys directionally solidified under unsteady-state conditions, Metallurg. Mater. Transact. A 39 (2008) 1712–1726, https://doi.org/10.1007/s11661-008-9536-z.
[41] A. Zhang, Y. Li, Thermal conductivity of aluminum alloys-a review, Materials 16 (8) (2023) 2972, https://doi.org/10.3390/ma16082972.
[42] R.A. Muriana, O.K. Abubakre, S.B. Tajiri, Effects of heat-treatments on tensile strength and electrical conductivity of locally formulated Al-Ni alloys, Int. J. Eng. Res. 4 (7) (2015) 384–388, https://doi.org/10.17950/ijer/v4s7/710.
[43] R. Brandt, G. Neuer, Electrical resistivity and thermal conductivity of pure aluminum and aluminum alloys up to and above the melting temperature, Int. J. Thermophys. 28 (5) (2007) 1429–1446, https://doi.org/10.1007/s10765-006-0144-0.